AUTHORS' POSTPRINT Originally published in AIP Conference Proceedings 1999, 040023 (2018);
https://doi.org/10.1063/1.5049286

Integrating Transparent Conductive Oxides to Improve the Infrared Response of Silicon Solar Cells with Passivating Rear Contacts

Leonard Tutsch[1, a)], Frank Feldmann[1], Martin Bivour[1], Winfried Wolke[1], Martin Hermle[1] and Jochen Rentsch[1]

[1]*Fraunhofer Institute for Solar Energy Systems, Heidenhofstrasse 2, 79110 Freiburg, Germany*

[a)]Corresponding author: leonard.tutsch@ise.fraunhofer.de

Abstract. This work addresses the development of a transparent conductive oxide (TCO)/metal stack for n-type Si solar cells featuring a tunnel oxide passivating rear contact (TOPCon). While poly-Si based passivating contacts contacted by local fire-through metallization currently show an increased recombination at the metal contacts and a poor infrared (IR) response, we aim to realize a full-area metallization which maintains the high level of surface passivation and avoids IR losses. Some research groups have reported that sputtering TCOs on poly-Si based passivating contacts degrades the surface passivation and unlike the SHJ cells this degradation cannot be cured completely at $T_{cure} \sim 200°C$. However, the higher thermal stability of TOPCon allows for higher T_{cure} of up to 400°C, which can effectively restore the surface passivation. On the other hand, the contact resistivity (ρ_c) of the TOPCon/ITO/metal contact increased by several orders of magnitude in our test structures during annealing at such high temperatures. Possible reasons like the formation of an interfacial oxide are currently under investigation. Increasing the poly-Si thickness and/or doping mitigated the effect of sputter damage, but this will come at the cost of more parasitic absorption. However, by adapting the sputter and the subsequent annealing process, we were able to realize low damage deposition of ITO (loss in implied $V_{oc} \sim 7$ mV) on thin, lowly doped poly-Si layers on textured wafers, yielding reasonable contact properties ($\rho_c \sim 40$ mΩcm² of the whole rear contact stack).

INTRODUCTION

Passivating contacts consisting of an ultra-thin SiO_x layer below a heavily doped silicon film (e.g. TOPCon [1]) have demonstrated very low recombination current densities (J_0) and the implementation at the rear of an n-type solar cell led to an efficiency of 25.8% [2,3]. While those results were achieved on small area lab cells, attempts to put similar concepts into practice for larger cells and by using industry-proven techniques still lowers the efficiency by several percent absolute (e.g. to < 22% for bifacial cells on 6" Cz wafers in [4]). In essence, LPCVD poly-Si contacts contacted by fire-through metallization become locally depassivated, due to the penetration of metal through the poly-Si layer into the c-Si absorber ($J_{0,met} \gg J_{0,pass}$ [5,6]). Reasonable $J_{0,met}$ and contact resistivity (ρ_c) values can be achieved for heavily-doped, thick poly-Si films, but here the IR response is reduced noticeably due to free carrier absorption (FCA). In this paper, we focus on low-damage sputter deposition of ITO on thin PECVD poly-Si contacts [7–11] with the purpose to realize an optical spacer preventing surface plasmon absorption within the subsequent metal [12]. Successively sputtering of a TCO/metal stack is an economically attractive option for the rear metallization of a monofacial cell with (i) passivation quality, (ii) electrical contact properties and (iii) infrared response being important design parameters. This work considers these three aspects and tries to find solutions to combine them e.g. in n-type cells with passivating electron rear contact [2]. Furthermore, investigating a marginally damaging TCO deposition procedure with suitable contact properties on top of thin, moderately doped poly-Si is obviously also important for its integration at the front side and / or for bifacial cells providing lateral conductivity with lower parasitic absorption, compared e.g. to well-conductive poly-Si films.

EXPERIMENTAL DETAILS

To characterize the rear contact in terms of passivation quality, electrical contact resistance and IR response, TOPCon test structures were coated with ITO by DC magnetron sputtering in a high rate process performed by a tool designed to coat industrially sized wafers at high throughput. A circular ITO target with a composition of In_2O_3/SnO_2: 90/10 weight percent, a diameter of 30 cm and a purity of 99.99 % was utilized and additional oxygen was introduced along with argon during the sputter process, which dosage allows for controlling the density of electrons in the conduction band of the deposited film.

The sputter-induced damage of well-passivated lifetime samples was evaluated via photo conductance measured by the Sinton WCT-120 tool operated in generalized mode [13] and quantified by the corresponding iV_{oc} values at one sun illumination averaged for at least two samples. The TOPCon lifetime samples consisted of 200 µm thick n-type silicon FZ wafers with a resistivity of 1 Ωcm (Fig. 1a and Fig. 2) or 10 Ωcm (Fig. 1b) possessing either planar surfaces or a random pyramid texture etched in alkaline solution. After growing an ultrathin SiO_x layer, amorphous silicon of varying doping concentration and thickness was deposited by means of direct plasma PECVD and then crystallized in a tube furnace before receiving hydrogen passivation (for details of the TOPCon process sequence see [7]).

The contact resistivity of the whole TOPCon/ITO/Ag rear contact layer stack was determined from dark I-V-measurements through a symmetrically coated planar wafer ($R_{total} = R_{base} + 2 \times R_c$). To prevent current crowding in the locally contacted structure and thus to ensure a homogeneous 1D current flow through the interfaces, the ρ_c samples were broken into 5x5 mm² squares after deposition.

For examining the IR reflection at the rear side of the cell, on both sides textured c-Si wafers with SiN_x anti-reflection coating on the front side and a TOPCon/ITO/Ag stack on the rear were used.

The bulk charge carrier density and DC mobility of the here applied ITO thin films were determined by Hall measurements via the Van der Pauw method for 100 nm thick films deposited on glass.

RESULTS AND DISCUSSION

Influence of Poly-Si Doping and Thickness on Sputter-Induced Degradation and Contact Resistivity

Firstly, the impact of ITO deposition on the absorber surface passivation provided by TOPCon was studied. The applied power during the DC sputter process was 2.5 kW and a relatively high chamber pressure of 17 µbar was present, since this has been observed to reduce the sputter impact on the passivation quality. Here introducing an oxygen flow of 1 % of the argon flow yielded the best electrical bulk properties of the ITO film. Fig. 1a (left axis) shows the implied V_{oc} of planar lifetime samples with 35 nm thick poly-Si layers after hydrogen passivation as well as after the sputter process for three doping profiles, adjusted by the phosphine flow during the a-Si deposition. The initial iV_{oc} decreased with doping from 731 mV to 698 mV potentially due to an increased Auger recombination rate in the silicon absorber induced by stronger phosphor diffusion into the wafer [10,14]. Conversely the sensitivity to sputter damage decreased, resulting in a similar post-sputter iV_{oc} level of 720 mV for low and moderate doping. This can also likely be attributed to the increased diffusion of the n-type dopants, spatially shielding the minority carriers (holes) away from the emerging recombination active states at the interface. The related contact resistivities (right axis) decrease slightly with poly-Si doping, but since they are all on a low level of < 10 mΩcm², any of the considered doping profiles would allow for high fill factors when applied to solar cells with full-area rear contacts. Owing to the preceding process chains conventionally used in industry or due to intentional etching to improve the optics, the wafer surface on the rear side is usually not planar. Furthermore the poly-Si thickness should be reduced in order to prevent significant parasitic absorption. Both can result in a far more sensitive interface passivation as can be seen in Fig. 1b for a random pyramid texture. The degradation of the initially high iV_{oc} values (724 mV – 727 mV) is shown for 15 nm thick poly-Si deposited at a PH_3 flow of 1000 sccm and 1500 sccm, as well as for double the thickness (30 nm, 1000 sccm PH_3). In order to estimate the poly-Si thickness on textured surfaces, the film thickness on planar control samples, obtained by ellipsometry, was multiplied by a factor of 0.7. Although the damage was severe for all samples (iV_{oc} < 700 mV), the previously mentioned effect for higher doping could again be observed. Also increasing the poly-Si layer thickness resulted in a reduced degradation, since high energy particles bombarding the substrate as well as plasma radiation, both emerging during the sputter process and being mainly responsible for the sputter damage (similar to what was reported for hydrogenated amorphous Si based passivation [15]), could be shielded more

effectively from the c-Si/SiO_x interface region. However, in order to recover the initial iV_{oc} level, a post-sputter thermal curing step is indispensable for any of the here applied poly-Si doping and thickness in case of textured interfaces.

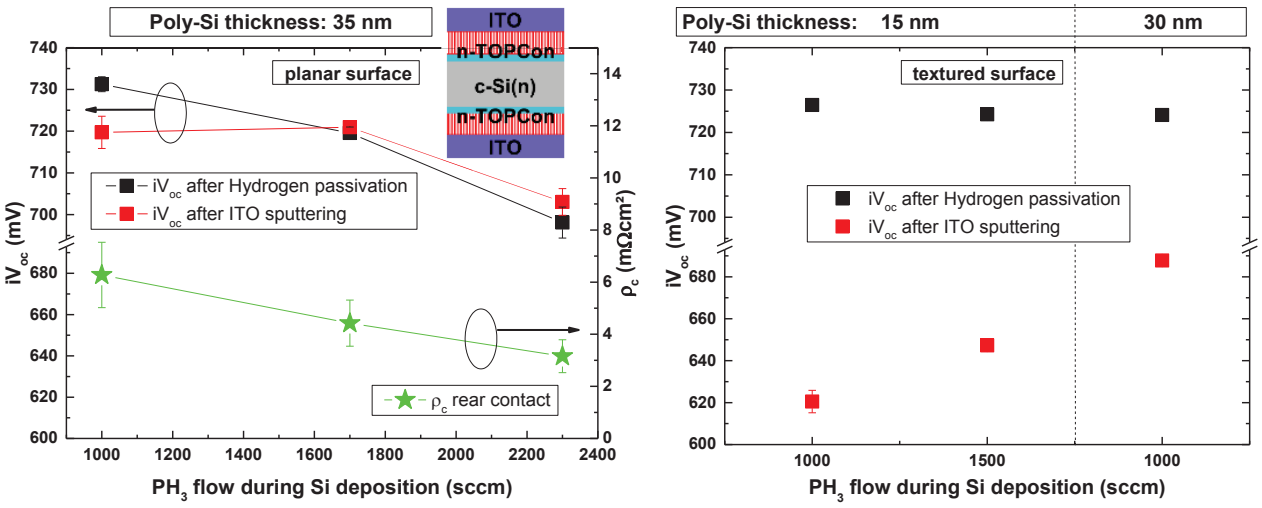

(a) (b)

FIGURE 1. Sputter-induced degradation of the passivation quality dependent on surface morphology and poly-silicon doping concentration and thickness together with the corresponding contact resistivity.

Thermal Curing of the Interface Passivation and its Impact on the Contact Resistivity

To regain the initial high level of interface passivation after the sputter process, textured lifetime samples containing a 22 nm thick lowly doped poly-Si layer were annealed in ambient air on a hotplate (Fig. 2b). Considering that the poly-Si thickness was in between 15 nm and 30 nm here, the average post-sputter iV_{oc} of 707 mV was higher than expected from the previous experiment (Fig. 1b). The passivation could be restored almost completely ($\Delta iV_{oc} < 3$ mV) at 350°C. Interestingly, for the adjusted sputter process applied here, the original level could also be approached after thermal treatment at 250°C ($\Delta iV_{oc} \sim 7$ mV). At both temperatures, a variation of the curing time (not depicted) between 3 and 15 minutes showed no statistically significant effect on ΔiV_{oc}.

Planar test structures for a quantification of the related contact resistivity of the TOPCon/ITO/Ag rear received the same TCO process and an analogous temperature treatment after being coated with silver. The hereby emerging temporal evolution of ρ_c (Fig. 2a) is presented for curing at 250°C and 350°C. The low post-sputter ρ_c of ~ 20 mΩcm² was slightly higher than in the previous experiment (Fig. 1a), likely due to minor changes in the process sequence. While ρ_c only slowly increased with time to around 40 mΩcm² at 250°C, the contact resistivity diverged at 350°C, already exceeding 1 Ωcm² after 1 minute of curing. Although shorter annealing durations should be investigated for a better understanding of the timescale of curing and contact barrier formation at 350°C, the rapidly increasing ρ_c makes conventional annealing in ambient air unsuitable at this temperature. In contrast, a thermal treatment at lower temperatures of around 250°C could combine significant curing of the interface passivation together with adequate electrical contact properties of the rear contact, allowing high V_{oc} and FF, respectively.

Fig. 3 shows the electrical bulk properties of ITO films, which initially exhibited a low (green), moderate (red) and high (black) electron concentration N_e within the conduction band, by means of altering the oxygen addition during the sputter process, determining the amount of electron donating oxygen vacancies within the TCO. The Hall mobility μ peaked at $N_e \sim 10^{20}$ cm^{-3}, due to an optimum in the average time between scattering events induced by potential barriers – dominant mechanism for lower N_e – and ionized impurities – limiting μ at higher N_e [16]. During the annealing steps, where the films crystallized partially while being exposed to ambient air, the N_e of the three ITO layers converged to ~ 10^{20} cm^{-3}. Beyond that an improvement and degradation of μ took place at 250°C and 350°C, respectively. Even though there are little requirements for the lateral conductivity of the TCO in a full-area metallized contact, N_e can have an influence on the width of a potentially arising electrical contact barrier at its interfaces [17]. Furthermore N_e together with the optical mobility (not necessarily comparable to the here measured DC mobility) determine the free carrier absorption according to the Drude model [18] and thus the infrared response of the rear side of the cell.

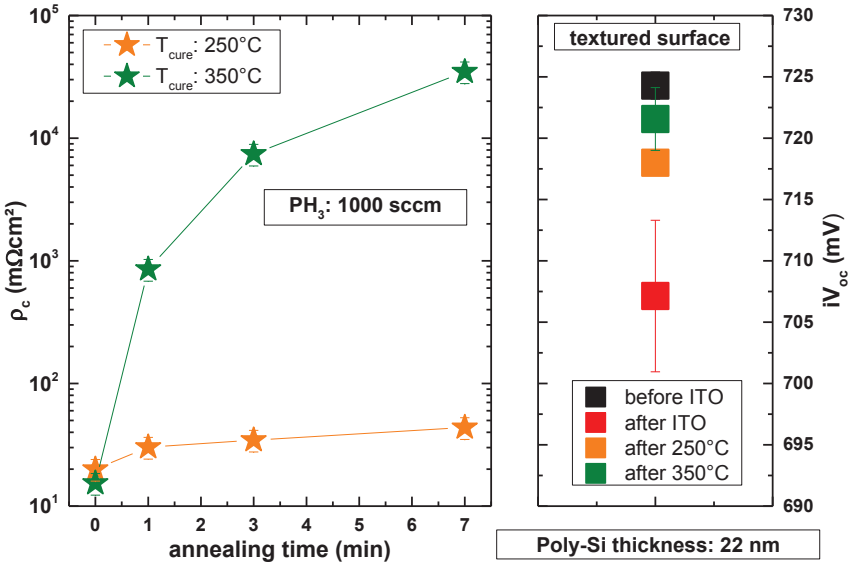

FIGURE 2. Evolution of ρ_c (a) and iV_{oc} (b) under thermal treatments conducted at 250°C and 350°C.

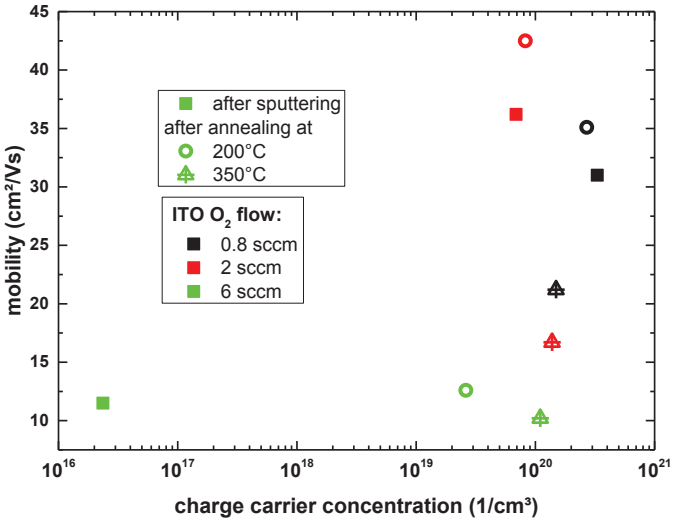

FIGURE 3. Hall mobility and concentration of charge carriers in ITO.

Optical Performance of Differently Doped ITO as Spacing Layer in the Rear Contact

A clear benefit of inserting a TCO layer as optical spacer is depicted in Fig. 4, where 0, 50, 100 and 150 nm thick ITO interlayers with different electron densities (shown in Fig. 3) were sputtered on both side textured reflection samples between poly-Si and silver. Silicon nitride is deposited as anti-reflection coating on the front side of the wafer. For the highly doped ITO (black lines), the infrared reflection was worse than for the bare silver reference (blue), likely due to the large FCA in this layer. The moderately (red) and lowly (green) doped films yielded a significant improvement of the IR response. A minimum ITO thickness of 100 nm was necessary to shield the evanescent light waves sufficiently from the absorbing metal. Reflection curves measured after annealing at 250°C behaved very

similar compared to before annealing (Fig. 4b). Here the influence of a silver capping on the electrical properties N_e and μ of the ITO films during annealing has to be investigated and linked to the optical data. The improved IR response was still present after a further thermal treatment at 350°C (not shown), whereby the reflection converged slightly for the different ITO films, which is likely linked to a converging carrier density.

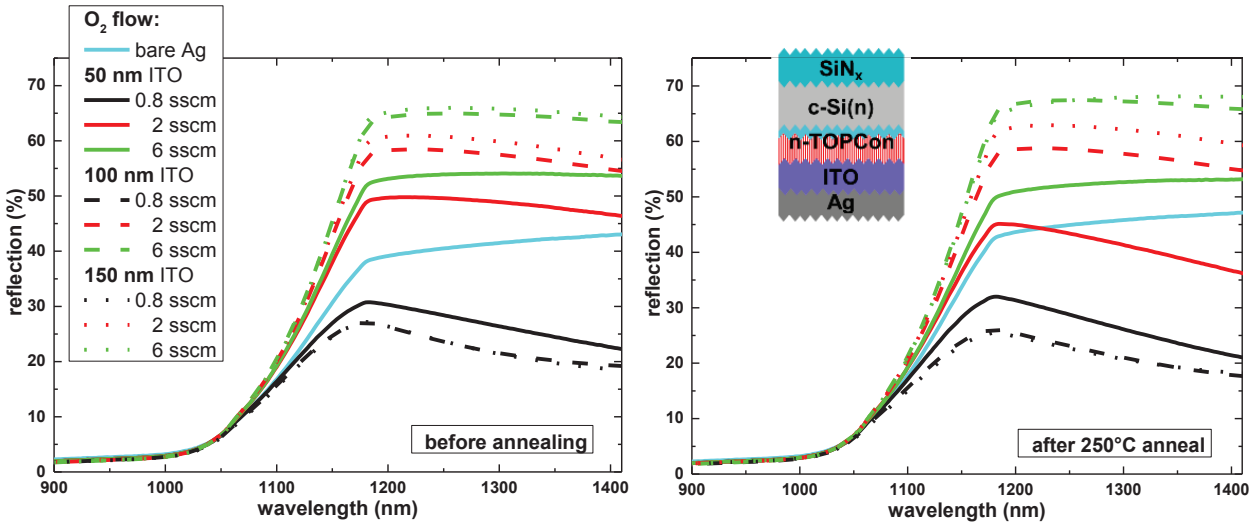

(a) (b)

FIGURE 4. Infrared reflection of textured samples with poly-Si/ITO/Ag rear before (a) and after (b) annealing.

CONCLUSION

After being degraded by DC magnetron sputtering, the surface passivation quality of TOPCon could be cured in a 350°C annealing step. While the iV_{oc} was thereby restored even for textured samples containing only 22 nm thin poly-Si layers, the electrical contact resistivity deteriorated after being at an initially suitable value of < 20 mΩcm². Increasing the thickness of the poly-Si layer and / or its doping level could ease this trade-off. Here, by varying the phosphorus concentration in the a-Si / poly-Si and thus the diffusion profile in the wafer, a partial transition of the wafer surface region from transparent to opaque for minority carriers (holes) could be observed in the varying sensitivity of the recombination current to sputter damage. However, increasing poly-Si thickness or doping comes at the cost of an increased FCA, leading to a loss in IR response and thus in J_{sc} of a corresponding cell.

An auspicious way to accomplish an effective curing ($\Delta iV_{oc} \sim 7$ mV) by simultaneously preserving an applicable contact resistivity of around 40 mΩcm², enabling a high FF, was found by decreasing the annealing temperature to 250°C. There is still room for improvement by optimizing the annealing temperature, duration and possibly atmosphere.

The optical performance of textured passivating rear contact test structures could be improved by the introduction of an ITO film as optical spacer between poly-Si and silver, effectively preventing surface plasmon absorption in the metal for TCO thicknesses ≥ 100 nm. Here the IR response of the reflection samples increased compared to the bare silver rear, as far as the charge carrier concentration and thus the FCA in the TCO was kept sufficiently low. This improvement was still present after annealing at 250°C, which only had a marginal impact on the optical performance.

ACKNOWLEDGMENTS

The authors would like to thank R. Sharma, J. Polzin, F. Schätzle, A. Seiler, K. Zimmermann, F. Martin and A. Leimenstoll for sample preparation and technical assistance.

This work was funded by the German Federal Ministry for Economic Affairs and Energy under contract number 03225877D (PROJECT PEPPER) and this project has received funding from the European Union's Horizon 2020 research and innovation programme under grant agreement No 727529 (PROJECT DISC).

REFERENCES

1. F. Feldmann, M. Bivour, C. Reichel, M. Hermle, and S. W. Glunz, Solar Energy Materials and Solar Cells **120**, 270 (2014).
2. A. Richter, J. Benick, F. Feldmann, A. Fell, M. Hermle, and S. W. Glunz, Solar Energy Materials and Solar Cells **173**, 96 (2017).
3. M. A. Green, Y. Hishikawa, E. D. Dunlop, D. H. Levi, J. Hohl-Ebinger, and A. W.Y. Ho-Baillie, Prog Photovolt Res Appl **26**, 3 (2018).
4. M. K. Stodolny, J. Anker, B. L.J. Geerligs, G. J.M. Janssen, B. W.H. van de Loo, J. Melskens, R. Santbergen, O. Isabella, J. Schmitz, M. Lenes, J.-M. Luchies, W. M.M. Kessels, and I. Romijn, Energy Procedia **124**, 635 (2017).
5. H. E. Çiftpınar, M. K. Stodolny, Y. Wu, G. J.M. Janssen, J. Löffler, J. Schmitz, M. Lenes, J.-M. Luchies, and L. J. Geerligs, Energy Procedia **124**, 851 (2017).
6. S. Mack, J. Schube, T. Fellmeth, F. Feldmann, M. Lenes, and J.-M. Luchies, Phys. Status Solidi RRL **11**, 1700334 (2017).
7. F. Feldmann, M. Simon, M. Bivour, C. Reichel, M. Hermle, and S. W. Glunz, Appl. Phys. Lett. **104**, 181105 (2014).
8. F. Feldmann, K.-U. Ritzau, M. Bivour, A. Moldovan, S. Modi, J. Temmler, M. Hermle, and S. W. Glunz, Energy Procedia **77**, 263 (2015).
9. G. Nogay, J. Stuckelberger, P. Wyss, E. Rucavado, C. Allebé, T. Koida, M. Morales-Masis, M. Despeisse, F.-J. Haug, P. Löper, and C. Ballif, Solar Energy Materials and Solar Cells **173**, 18 (2017).
10. J. Stuckelberger, G. Nogay, P. Wyss, A. Ingenito, C. Allebe, J. Horzel, B. A. Kamino, M. Despeisse, F.-J. Haug, P. Loper, and C. Ballif, IEEE J. Photovoltaics **8**, 389 (2018).
11. R. Peibst, Y. Larionova, S. Reiter, N. Orlowski, S. Schäfer, M. Turcu, B. Min, R. Brendel, D. Tetzlaff, J. Krügener, T. Wietler, U. Höhne, J.-D. Kähler, H. Mehlich, and S. Frigge, in 33rd European PV Solar Energy Conference and Exhibition, Amsterdam (2017).
12. Z. C. Holman, M. Filipič, A. Descoeudres, S. de Wolf, F. Smole, M. Topič, and C. Ballif, Journal of Applied Physics **113**, 13107 (2013).
13. H. Nagel, C. Berge, and A. G. Aberle, Journal of Applied Physics **86**, 6218 (1999).
14. F. Feldmann, R. Müller, C. Reichel, and M. Hermle, Phys. Status Solidi RRL **08**, 767 (2014).
15. B. Demaurex, S. de Wolf, A. Descoeudres, Z. Charles Holman, and C. Ballif, Appl. Phys. Lett. **101**, 171604 (2012).
16. K. Ellmer and R. Mientus, Thin Solid Films **516**, 4620 (2008).
17. A. Yu, Microelectronics Reliability **9**, 461 (1970).
18. H. Fujiwara and M. Kondo, Phys. Rev. B **71** (2005).